INS and IR and NMR Spectroscopic Study of C_1-C_4 Alcohols Adsorbed on Alkali Metal-Exchanged Zeolite X

Renate Schenkel,[†] Andreas Jentys,*[,†] Stewart F. Parker,[‡] and Johannes A. Lercher[†]

Institut für Technische Chemie, Technische Universität München, 85747 Garching, Germany, and ISIS Facility, Rutherford Appleton Laboratory, Chilton, Didcot, Oxon OX11 0QX, United Kingdom

Received: May 10, 2004; In Final Form: July 9, 2004

The adsorption of short-chain (C_1-C_4) *n*-alcohols on alkali cation-exchanged X zeolites (Si/Al = 1.2) was studied by inelastic neutron scattering and infrared and NMR spectroscopy. Vibrational and NMR spectra of alcohols adsorbed on the zeolites were compared to those of solid alcohols and isolated alcohol molecules to describe the interactions between the sorbate molecule and the zeolite. The experimental results are compared to theoretically calculated INS spectra for one, two, and three alcohol molecule aggregates. For all alkali-metal cation-exchanged X zeolites, only physically adsorbed alcohol molecules were found on the catalyst's surface. The interactions in the channels of alkali cation-exchanged X zeolites of the short-chain C_1-C_4 alcohols were found to be similar and independent of the chain length. The alcohol oxygen atoms interact via their lone electron pairs with the exchanged alkali-metal cation, and hydrogen-bond formation was found between the alcohol OH protons and the negatively charged oxygen atoms of the framework. With increasing hydrocarbon chain length, the energetic contribution of the hydrogen bonds to the heat of adsorption increased. With increasing framework polarity, that is, from the Na^+ to Cs^+ countercation, large negative shifts of the frequency of the OH stretching modes indicate the strengthening of the hydrogen bonds.

Introduction

Alkali-metal cation-exchanged zeolites are materials combining Lewis-acid and -base functionalities.[1] The Lewis acid sites are formed by the extraframework cations, whereas the negatively charged framework oxygen atoms of the zeolite have Lewis-base character.[2,3] The concentration of extraframework cations and, thus, the concentration of acid−base sites increase with the concentration of framework aluminum atoms occupying tetravalent cation positions (T sites) in the zeolite lattice. The base strength of framework oxygen sites adjacent to cations can be modified by changing the type of cation and increases in the order $Li^+ < Na^+ < K^+ < Rb^+ < Cs$.[4] Zeolites with basic functionality can be used to substitute for corrosive liquid bases in chemical processes.[5,6] The importance of basic sites in zeolites has been confirmed for numerous catalytic reactions,[7−10] among which the side-chain alkylation of toluene with methanol was one of the first clearly demonstrating the possibility of base-catalyzed reactions with zeolites.[8,10]

For the adsorption of methanol on (aluminum-rich) alkali cation-exchanged X zeolites, three local adsorption structures were identified:[11] (i) interaction between the alkali-metal cations (electron pair acceptor) and the methanol oxygen atoms (electron-pair donor), (ii) lateral interactions between the alcohol molecules via hydroxyl and methyl hydrogen atoms and the framework oxygen atoms, and (iii) intermolecular interactions between neighboring (adsorbed) molecules with the formation of ringlike hydrogen-bonded structures (Figure 1). The strength of the hydrogen-bonding interactions and the basicity of the framework oxygen atoms can be studied from the broadening and the change in the energy of the alcohol OH stretching and bending vibrations relative to their gas-phase values.[12]

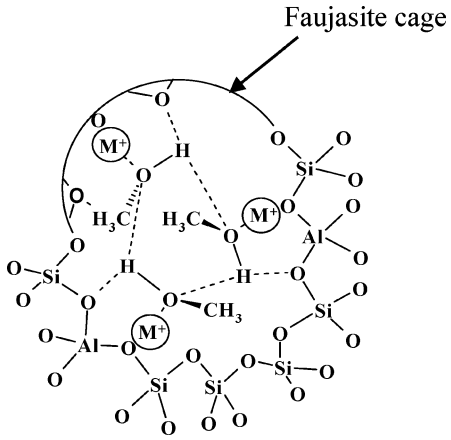

Figure 1. Schematic presentation of the interaction of methanol in aluminum-rich zeolites: hydrogen bonding between the methanol OH group and the lattice oxygen (3460 cm^{-1}; see text) and additional lateral interaction between adsorbed methanol molecules, as found for Na−X (3340 cm^{-1}; see text).

Self-association through hydrogen bonding was observed for primary alcohol molecules in the liquid state and was reported to be the main reason for the deviation from ideal behavior for mixtures of 1-alcohols and *n*-alkanes.[13] It is interesting that methanol dimers form linear structures but larger hydrogen-bonded clusters $(H_2O)_n$, $(CH_3OH)_n$, and $(C_2H_5OH)_n$, with *n* ranging up to 17, have cyclic and closed-ring structures.[14,15] However, evidence for chains was also found for liquid and solid methanol.[16,17] The existence of intermolecular structural associations via hydrogen bonding was also confirmed for liquid and solid ethanol.[18−20]

* Corresponding author. E-mail: andreas.jentys@ch.tum.de.
† Technische Universität München.
‡ Rutherford Appleton Laboratory.

10.1021/jp047998v CCC: $27.50
Published on Web 08/26/2004

TABLE 1: Characteristics of Alkali Metal Cation-Exchanged X Zeolites Determined from AAS Analysis and N_2 Sorption

sample	Si/Al	M^+/Al (mol %)	Na^+/Al (mol %)	unit cell composition	micropore volume (m^3/g)	S_{int}[a]	$-\delta_0$[b]	e/r[c] ($Å^{-1}$)
Na−X	1.2	100	100	$Na_{88}\,Al_{88}\,Si_{104}\,O_{384}$	0.17	2.314	0.337	1.05
K−X	1.3	95.3	2.3	$K_{82}\,Na_2\,Al_{84}\,Si_{108}\,O_{384}$	0.15	2.298	0.341	0.75
Rb−X	1.2	67.5	32.5	$Rb_{60}\,Na_{29}\,Al_{88}\,Si_{104}\,O_{384}$	0.11	2.232	0.358	0.67
Cs−X	1.3	55.4	44.6	$Cs_{47}\,Na_{38}\,Al_{84}\,Si_{108}\,O_{384}$	0.10	2.239	0.356	0.59

[a] $S_{int} = (S_P{}^p S_Q{}^q S_R{}^r S_T{}^t)^{1/(p+q+r+t)}$: for a compound $P_pQ_qR_rT_t$ calculated intermediate Sanderson electronegativity.[84,85] [b] Calculated average charge $-\delta_o$ on the oxygen of the lattice using $(S_{int} - S_o)2.08S_o^{1/2}$. [c] Electrostatic potential of the sodium cation (e/r).

In the present work, the nonreactive sorption of the short-chain aliphatic alcohols (methanol, ethanol, 1-propanol, and 1-butanol) on alkali cation-exchanged X zeolites is investigated by a combination of inelastic neutron scattering (INS), infrared (IR) spectroscopy, ^{1}H MAS NMR spectra, and temperature-programmed desorption. INS is complementary to infrared spectroscopy because it allows for the accessing of all vibrations of the molecules in the low-frequency region without limitations due to low transmittance of the samples and selection rules. Because INS is highly sensitive to the vibrational motions of the hydrogen atoms, it enables discrimination between vibrational modes of the adsorbate and the (non-H-containing) host material.[21] Overtones and combinations are allowed transitions in INS within the harmonic approximation. In particular, combinations (phonon wings) between the internal modes and the lattice modes occur. Their importance lies in the fact that the total spectral intensity is distributed between the internal mode and the phonon wing. Their intensity is determined by the momentum transfer (Q), which for the spectrometer used increases with the energy transfer (E) as $Q^2 \approx E/16$. Hence, at large energy transfer (>1600 cm^{-1}), most of the intensity occurs in the phonon wing, and the fundamental modes are not observed. In contrast, IR spectroscopy can readily access the wavenumber region above 1300 cm^{-1} with good resolution. Thus, the two methods provide complementary information about the molecules adsorbed, and the combination is a powerful approach for studying hydrogen-bonding interactions.[22−25] The influence of the increasing chain length of the alcohol molecules and the framework polarity on the sorption structure will be discussed. The interpretation of the spectra of the alcohol in the solid and the adsorbed state is supported by theoretical calculations of the vibrational modes of single alcohol molecules and aggregates of two and three molecules.

Experimental Section

Materials. Commercial Na−X zeolite (Köstrolith) was cation exchanged by liquid-phase ion exchange in 0.1 M aqueous alkali-metal nitrate solutions (Na^+, K^+, Rb^+, and Cs^+). The chemical composition (Si/Al ratio) of all materials was determined by atomic absorption spectroscopy (AAS, UNICAM 939), and the structural integrity was verified by powder X-ray diffraction (recorded with a Philips XPERT PRO diffractometer using the Cu Kα line) and nitrogen sorption isotherms (measured with a PMI sorptometer). The results are compiled in Table 1. Methanol, ethanol, 1-propanol, and 1-butanol (purity is p.a. $>$99.5%) were obtained from Merck AG and used without further purification.

INS Experiments and Sample Preparation. Inelastic neutron scattering measurements were performed on the spectrometer TOSCA at the spallation neutron source ISIS (Rutherford Appleton Laboratory, U.K.). TOSCA is an indirect geometry time-of-flight spectrometer that allows INS spectra in the energy-transfer range of 30−4000 cm^{-1} to be obtained with a resolution of $\sim$1.5% of the energy transfer.[26]

The partial pressure of the alcohol molecules during sorption on the alkali metal-exchanged zeolite X samples was adjusted to reach a loading of three molecules per supercage (coverage 0.27% with respect to the countercations). The activation, sorption, and sample preparation for the INS and IR experiments followed the procedures described in ref 27. The spectra of the solid alcohols were collected in flat, thin-walled aluminum cells. The INS spectra were recorded after cooling the sample containers below 20 K in a helium cryostat. Measurement times were typically approximately 10 h. The spectrum of an empty container and the activated zeolite was subtracted from the spectra of the samples in all data presented. Dehydrated zeolite samples are generally weak neutron scatterers; therefore, all intensity observed after the sorption in INS results from the H atoms in the sorbate molecules.

IR Spectroscopy. In situ IR spectra (Bruker IFS-88, resolution 4 cm^{-1}, base pressure below 10^{-6} mbar) were recorded at 308 K and at partial pressures from 10^{-3}−1 mbar[27] in the transmission absorption mode. The equilibration of the zeolite with the sorbate was time-resolved monitored. All spectra were baseline corrected between 3800 and 1200 cm^{-1} and normalized to the integral peak area of the overtone vibrations of the framework in the range between 2100 and 1735 cm^{-1}. The spectra presented in this paper are the difference between the spectra of the sample in contact with the alcohol molecules and the spectrum of the activated zeolite. In this mode of presentation, IR bands pointing upward increased in intensity, and bands pointing downward decreased in intensity as a result of the interaction of the zeolite with the sorbate molecules.

Computational Methods. The structure of single alcohol molecules and clusters consisting of two and three alcohol molecules (on clusters without including the interaction with the zeolite) were optimized with respect to the total energy using density functional theory methods (DFT) implemented in Gaussian 98 [28]. The 6-31G** basis set and nonlocal corrections on the B3LYP level were applied. After having achieved the optimized geometry for the different clusters, the vibrational modes were calculated. The displacement vectors determined for each vibrational mode were used to simulate the INS (including phonon wings and overtone vibrations) using the program CLIMAX.[29]

Temperature-Programmed Desorption Studies (TPD). Temperature-programmed desorption experiments were carried out in a quartz sample holder connected to a UHV chamber using a mass spectrometer (Balzers QMG 420) to detect the molecules desorbing. About 30−50 mg of zeolite powder was activated in vacuum ($p < 10^{-3}$ mbar) at 723 K (rate 10 K/min) for 1 h. After cooling to 308 K, the sample was exposed to the sorbate molecules at a partial pressure of 10 mbar. After evacuation for 1 h at 308 K to remove weakly physisorbed molecules, the TPD was recorded between 308 and 873 K with an increment of 10 K·min^{-1}.

NMR Spectroscopy. ^{1}H MAS NMR spectra were measured at 500 MHz using a Bruker 500 TM Ultrashield NMR

TABLE 2: Experimental Vibrational Frequencies, Assignments of the INS Bands of Methanol in the Solid and Adsorbed (Three Methanol Molecules per Faujasite Supercage, on Average) State (T < 20 K), and Theoretical Vibrational Frequencies of Methanol Clusters Calculated by DFT

DFT				INS	
monomer	linear dimer	cyclic trimer	assignment[a,b]	solid	ads on Na−X
1530 sh	1530 sh	1530, 1505	$\delta_{as}(CH_3)$	1446 br	1446 br
1505	1505	1490	$\delta_{s}(CH_3)$		
1386	1445 HB, 1373	1464, 1445	$\delta(OH)_{ip}$		
1179	1182	1184, 1136	$\delta(CH_3)_{rock}$	1149,	1158,
1095, 1062	1127 HB, 1082	1175, 1141, 1128	$\delta(CH_3)_{rock} + \delta(OH)_{ip}$	1123	1114
1083	1089 HB, 1056 w	1090 w, 1073	ν(CO)		
	730 HB	964, 785, 732	$\delta(OH)_{op}$	773, 697	900−600 br
340	332		$\delta(OH)_{op}$		
	218	240, 232, 218	OH···H stretch	220	90 br + tail
	137	173, 124, 121, 116,	τ (CH_3)	166	
	109, 87, 72, 44	109, 97, 59, 52, 44	intermolecular	110 s	

[a] All frequencies are in cm^{-1}; vs = very strong, s = strong, m = medium, w = weak, vw = very weak, sh = shoulder, br = broad, and d = H-donor molecule. [b] aCLIMAX fit to methanol DFT data.

spectrometer at room temperature. ZrO_2 rotors of 4-mm size were filled under a nitrogen atmosphere with alcohol (three alcohol molecules per faujasite supercage)-loaded Na−X zeolite samples. The experiments were carried out by single-pulse excitation (SPE) in a magnetic field of 11.75 T. The rotation frequency was 14 kHz, and the chemical shifts were measured relative to adamantan (2.0 ppm for ^{1}H) as an external reference. ^{1}H NMR spectra of liquid and diluted C_1-C_4 alcohols were measured at 360 MHz using a Bruker AV 360 NMR spectrometer at room temperature. The experiments were carried out in a magnetic field of 8.46 T, and the chemical shifts were measured relative to CCl_3D (7.24 ppm).

Results

Inelastic Neutron Scattering Studies. The observed and calculated frequencies for the C_1-C_4 alcohols (methanol, ethanol, 1-propanol, and 1-butanol) in the range of 30−2000 cm^{-1} are listed in Tables 2−5. The experimental and calculated INS spectra of the different alcohols are shown in Figures 2, 3, 5, and 7 for methanol, ethanol, 1-propanol, and 1-butanol, respectively. (The spectrum of the dehydrated zeolite[27] and the empty cell was subtracted from all spectra shown.) The assignment of the vibrational frequencies in the spectra of the solid alcohol molecules and the alcohol molecules adsorbed on Na−X is based on comparisons with vibrational assignments reported for methanol,[16,30,31] ethanol,[32−35] 1-propanol,[36,37] and 1-butanol[38,39] as well as on the results of the ab initio calculations carried out for monomers and linear dimer and cyclic trimer clusters.[40,41]

Methanol has only 1 energetically stable geometry, but ethanol has 2 and 1-propanol has 5, and in 1-butanol 14 conformers exist. In all calculations, a staggered conformation of the C−C bonds was used for the alcohol molecules. The calculation of the INS spectra of the ethanol and 1-propanol monomer (M) was performed for the all-trans (t, T) conformation (M_t and M_{Tt}, respectively), where the CCOH and CCCO dihedral angles are equal to 180° and the terminal methyl and ethyl groups are in the trans (t) position with respect to the hydroxyl group. In the linear dimer (D) cluster, both ethanol molecules were in the gauche (g′) conformation ($D_{g'g'}$) with a CCOH dihedral angle of about 300° (Figure 4). Both 1-propanol molecules were in the Tg′ conformation ($D_{Tg'\ Tg'}$) in the dimer cluster, whereas for the trimer (T) cluster, the molecules were in the Tg, Gg′, and Gt conformation ($T_{Tg\ Gg'\ Gt}$) (Figure 6). The 1-butanol monomer was in the TTg′ conformation, and for the dimer cluster, the 1-butanol molecules were oriented in the $D_{GTg'GTt}$ conformation with the donor molecule in the DTg′ form (Figure 8). Note that for the C_1-C_4 alcohols trans as well as gauche isomers were found in the gas phase,[42] but the trans conformer of ethanol that was suspended in argon matrixes at 20 K was found to be more stable than the gauche conformer.[43] In crystalline ethanol, trans and gauche conformers were found to alternate, forming U-shaped chains.[44] Similar results were also shown by ab initio calculations[45] and microwave spectroscopy for gaseous and liquid ethanol and 1-propanol.[32,37,46]

Infrared Spectroscopy of C_1-C_4 Alcohols Adsorbed on Na−X. The changes in the IR spectra after the adsorption of the series of alcohols with a partial pressure of 1×10^{-3} mbar at 308 K on Na−X are shown in Figure 9. The bands of the adsorbed C_1-C_4 alcohol species are summarized together with their assignment (based on comparisons with literature data) in Table 6. The band of the OH stretching vibration ν(OH) of all sorbate molecules was strongly broadened and located at 3341 cm^{-1} with a shoulder at 3460 cm^{-1}. With increasing hydrocarbon chain length, a slight decrease of the ν(OH) frequency was observed, and the intensity ratios of the hydrocarbon stretching vibrations in the region 3000−2840 cm^{-1} change because of the increasing number of CH_2 groups.

Temperature-Programmed Desorption. The strength of interaction between the *n*-alcohol molecules and the zeolites can be evaluated from the temperature of the desorption maxima in the TPD. Signals corresponding to molecularly adsorbed *n*-alcohols were observed by mass spectrometry. The rate of desorption of C_1 to C_4 *n*-alcohols adsorbed on K−X is shown in Figure 10. The temperature of the maximum in the desorption rate increased from C_1 to C_4 alcohols. Similar trends in the temperature of the maximum in the desorption rate were observed for the other alkali-metal cation-exchanged samples.

Solid- and Liquid-State NMR Investigations. The ^{1}H NMR spectra of linear C_1-C_4 alcohols adsorbed on Na−X are shown in Figure 11. The chemical shifts are listed in Table 7 together with results obtained for diluted C_1-C_4 alcohols (0.445 M in CCl_3D), pure liquid C_1 and C_4 alcohols, and CD_3OH adsorbed on a series of zeolites. In contrast to the pure liquid (which shows hydrogen-bound OH groups), the hydrogen bridges are not formed to a significant extent after dilution with CCl_3D.

The NMR resonances of diluted, pure, and adsorbed 1-butanol are shown in Figure 12. The OH resonance (arrow marked) appeared at 2.34 ppm for dilute butanol, at 5.73 ppm for the neat liquid, and at 6.82 ppm when adsorbed on NaX. The signal of butanol adsorbed on NaX was considerably broader than all

TABLE 3: Experimental Vibrational Frequencies, Assignments of the INS Bands of Ethanol in the Solid and Adsorbed (three ethanol molecules per faujasite supercage, on average) State (T < 20 K), and Theoretical Vibrational Frequencies of Ethanol Clusters Calculated by DFT

DFT		DFT		DFT		INS [a]	
monomer M_t	assignment[b]	linear dimer $D_{gg'}$	assignment[b]	cyclic trimer T_{tt} [49]	assignment[b]	solid [46,47]	ads on Na−X
1547	$\delta(CH_2)$	1535, 1531, 1513, 1508, 1506, 1504,	$\delta(CH)$	1526, 1528, 1500, 1485	$\delta(CH)$	1480 1457 1426 sh	1340−1700: 1485 1440
1514	$\delta(CH_3)$	1455 (d)	$\delta(COH)_{ip}$	1481, 1466, 1464	$\delta(COH)_{ip}$	1385 br	1390 sh
1490	$\delta(CH_2)_{twist}$	1424 (d)	$\delta(CH_2)_{wagg} + \delta(OH)_{ip}$	1405, 1404	$\delta(CH_3)$		1356 sh
1476	$\delta_{as}(CH_3)$	1434, 1412, 1401 (d)	$\delta_s(CH_3) + \delta(CH_2)_{wagg}$	1381, 1322, 1307	$\delta(CH_2)_{wagg} + \delta(OH)_{ip}$		
1470	$\delta(CH_2)_{wagg} + \delta(OH)_{ip}$	1380	$\delta(COH)_{ip}$	1301, 1300	$\delta(CH)_{rock}$	1286	1287, 1230
1413	$\delta_s(CH_3)$	1303 (d), 1295	$\delta(CH_2)_{twist} + \delta(COH)_{ip}$	1178, 1117, 1118	$\delta(CH)_{rock}$	1154 w 1132 w	1080−1200 1134
1304	$\delta(CH_2)_{twist}$	1154 (d), 1138	$\delta(CH)_{rock}$	1116, 1107	$\delta(CH_3)_{rock}$	1101	1095
1279 sh	$\delta(COH)_{ip}$	1138, 1115 (d)	$\delta(CH_3)_{rock} + \delta(COH)_{ip}$	1076, 1055, 1051	$\nu_{as}(CCO)$	1061 w	1052 w, sh
1190	$\delta(CH)_{rock}$	1081	$\nu_{as}(CCO) + \delta(CH_3)_{rock}$	900, 898, 896	$\nu_s(CCO)$	934 sh	942 w
1123	$\nu_{as}(CCO) + \delta(CH_3)_{rock}$	1076 (d), 1068	$\nu_{as}(CCO) + \delta(COH)_{ip}$	826, 820, 819	$\delta(CH_2)_{rock-twist}$	888 w, br, 809	880, 805
1037	$\nu_{as}(CCO) + \delta(COH)_{ip}$	894	$\nu_s(CCO) + \delta(CH_3)_{rock}$	809, 724, 628	$\delta(OH)_{op}$	715 w, br	640 w, br
909	$\nu_s(CCO) + \delta(CH_3)_{rock}$	813 (d), 810	$\delta(CH_2)_{rock-twist} + \delta(CH_3)_{rock}$	444, 436, 434	$\delta(CCO)$	430	436
826	$\delta(CH_2)_{rock-twist} + \delta(CH_3)_{rock}$	698 (d)	$\delta(OH)_{op}$	262, 261, 257	$\tau(CH_3)$	270[d]	276
416	$\delta(CCO)$	439, 421 (d)	$\delta(CCO)$		$\nu(OH\cdots O)$	240 sh	240 sh,
293	$\delta(OH)_{op}$	359	$\delta(OH)_{op}$		$\delta(OH\cdots O)$		184 w
249	$\tau(CH_3)$	281, 268 (d)	$\tau(CH_3)$				
		151, 97, 79, 42	intermolecular	173, 168, 161, 120, 80, 58, 54, 48, 44	intermolecular	93 br[d]	134, 122 sh, 101 sh, 66 s br

[a] All frequencies are in cm^{-1}; vs = very strong, s = strong, m = medium, w = weak, vw = very weak, sh = shoulder, br = broad, and d = H-donor molecule. [b] aCLIMAX fit to ethanol DFT data.

other signals. All spectra of the alcohols show only one signal for the OH, CH_2, and CH_3 groups.

For all alcohols, the strongest shift of the hydrocarbon protons was found for those in the α position, and with increasing distance of the CH groups from the oxygen atom, the resonances were located at lower frequencies. The CH resonances from groups at the same chain position were of similar value, whereas after adsorption, all CH_2/CH_3 resonances were shifted by about 1.3−1.4 ppm to the lower field compared to the ones in diluted alcohol solution. A weak increase of the chemical shift of the OH protons of adsorbed alcohols toward higher frequencies was observed with increasing hydrocarbon chain length, whereas the CH_3 proton resonances for C_2-C_4 alcohols were very similar.

Discussion

Solid Alcohols. *Torsional Vibration Modes.* The INS spectra of solid C_1-C_4 alcohols exhibit an increasing number of bands with increasing hydrocarbon chain length as the number of torsional modes of the hydrocarbon chain increases. Generally, an alcohol molecule with a hydrocarbon chain containing n carbon atoms has $n - 1$ torsional modes. There are $n - 2$ modes of the C−C bonds and one mode of the C−O bond.

Besides a broad band in the energy region below 200 cm^{-1}, corresponding mainly to the transversal acoustic modes (TAMs), the lower longitudinal acoustic modes (LAMs), and the external modes (typically observed for alkanes below 220 cm^{-1}),[47] the methyl torsion modes are also located in the low-frequency region. For all alcohols except methanol (166 cm^{-1}), the methyl torsion modes were observed between 230 and 270 cm^{-1}. Barnes et al.[43] reported a band at 264 cm^{-1} for ethanol in argon matrixes at 20 K and assigned it to either the methyl torsion or the OH out-of-plane mode of an open-chain multimer. Assuming the formation of hydrogen-bond interactions between the majority of the ethanol OH groups exists, which would cause a significant shift of the OH bands to higher frequencies, we assign the band at 270 cm^{-1} to the methyl torsional vibrations $\tau(CH_3)$. Note that for ethane, CH_3-CH_3, a torsional frequency of 275−280 cm^{-1} was reported from INS measurements.[47] For ethanol, the frequency of the methyl torsional modes (270 cm^{-1}) was higher compared to that of 1-propanol molecules (233 cm^{-1}), whereas for 1-butanol, the frequency (254 cm^{-1}) was identical to that of the alkane methyl vibrational mode (∼250 cm^{-1}).[47] These frequency variations are attributed to the change in the electron-withdrawing effect of the alcohol oxygen atom on the methylene−methyl bond.

For methanol, the methyl torsional vibration was found at very low frequencies (at 166 cm^{-1}).[27] Because of the direct neighborhood of the methyl group with respect to the oxygen atom, the methanol $C^{\alpha}-O$ bond is elongated, leading to a simplified torsion around this bond. With increasing carbon number, the withdrawing inductive effect of the hydroxyl group leads to a slightly reduced distance of the $C^{\alpha}-C^{\beta}$ bond, whereas the $C^{\beta}-C^{\gamma}$ bond length is similar to that of the C−C distances of alkanes.[13,48] Note that the presence of the OH group in linear alcohols was found to influence mainly the α-CH_2 group becasue it is in the same neighborhood as the hydroxyl group, whereas the other CH_2 groups were hardly affected.[49,50] The shortened $C^{\alpha}H_2-C^{\beta}H_3$ distance in ethanol further led to a more-hindered methyl torsional vibration, whereas the longer $C^{\beta}H_2-C^{\gamma}H_3$ distance of 1-propanol led to a less-hindered $\tau(CH_3)$. The inductive effect decreases with distance and is diminished for 1-butanol. Therefore, the C−C torsional and other modes without a contribution of the α-CH_2 group are expected at similar positions to that of the alkane;[47,51] moreover, similar

TABLE 4: Experimental Vibrational Frequencies, Assignments of the INS Bands of 1-Propanol in the Solid and Adsorbed (Three 1-Propanol Molecules per Faujasite Supercage, on Average) State (T < 20 K), and Theoretical Vibrational Frequencies of 1-propanol Clusters Calculated by DFT

DFT		DFT		DFT		INS[b]		
monomer M_{Tt}	assignment[a]	linear dimer $D_{Tg'Tg'}$	assignment[a]	cyclic trimer $T_{Tg\,Gg'\,Gt}$	assignment [a]	solid [33]	ads on Na−X	ads on Cs−X
1532, 1518, 1504	$\delta(CH_2)$	1519	δ(CH)	1525, 1520, 1518, 1509	δ(CH)		1800−1200: 1455, 1380	1800−1200: 1480, 1454
1514	$\delta_{as}(CH_3)$	1534 (d), 1532, 1509 (d), 1505	$\delta(CH_2)$	1501	$\delta(OH)_{ip} + \delta(CH_2)$			1415 sh, br, 1388
1435	$\delta(OH)_{ip} + \delta(CH_2)_{wagg}$	1516, 1514 (d)	$\delta_{as}(CH_3)$	1536 (C1) 1531, 1505, 1492	$\delta(CH_2)$			
1425	$\delta_s(CH_3) + \delta(CH_2)_{wagg}$	1459	$\delta(OH)_{ip}$	1515, 1511	$\delta_{as}(CH_3)$			
1398, 1254, 1149	$\delta(CH_2)_{wagg} + \delta(C-OH)_{ip}$	1437, 1429 (d)	$\delta(OH)_{ip} + \delta(CH_2)_{wagg}$	1461	$\delta(OH)_{ip}$	1455		
1340, 1320	$\delta(CH_2)_{wagg}$	1427	$\delta_s(CH_3) + \delta(CH_2)_{wagg}$	1495, 1474	$\delta(OH)_{ip} + \delta(CH_2)_{wagg}$			
1102	$\nu(CC) + \delta(CH_2)_{wagg}$	1424 (d),	$\delta_s(CH_3)_{umbrella}$	1432, 1430	$\delta(OH)_{ip} + \delta_s(CH_3) + \delta(CH_2)_{wagg}$			
1080	$\nu_{as}(CCO)$	1390	$\delta(C-OH)_{ip} + \delta(CH_2)_{twist} + \delta(CH_2)_{wagg}$	1427, 1424	$\delta_s(CH_3)_{umbrella}$	1425		
1035	ν(CC)	1344 (d), 1341	$\delta(CH_2)_{twist} + \delta(CH_3)_{rock}$	1430, 1412, 1388, 1386	$\delta_s(CH_3) + \delta(CH_2)_{wagg}$	1393		
895	$\delta\,(CH_2)_{twist} + \delta(CH)_{rock}$	1324 (d), 1322	$\delta(CH_2)_{twist}$	1367, 1304	$\delta(C-OH)_{ip} + \delta(CH_2)_{twist} + \delta(CH_2)_{wagg}$	1378		
890	$\delta(CH_3)_{rock} + \nu_s(CCO)$	1264 (d), 1253	$\delta(CH_2)_{twist} + \delta(C-OH)_{ip}$	1341	$\delta(CH_2)_{wagg} + \delta(CH_3)_{rock}$	1357 sh w	1351 sh	1358
764	$\delta(CH_2)_{rock}$	1158, 1120w	$\delta(CH_2)_{wagg} + \delta(C-OH)_{ip}$	1310	$\delta(CH_2)_{twist} + \delta(CH_3)_{rock}$			
459	δ (CCO)	1160 (d), 1148, 1100	$\delta(C-OH)_{ip} + \delta(CH_2)_{twist} + \delta(CH_3)_{rock}$	1329, 1280	$\delta(CH_2)_{twist}$	1295	1297	1286, 1303
328	$\delta\,(C-OH)_{op}$	1072 w	$\nu(CC) + \delta(CH_2)_{wagg}$	1269, 1265	$\delta(CH_2)_{twist} + \delta(C-OH)_{ip}$	1240	1237	1238, 1246
265	δ (CCC)	1095 (d), 1070 w	$\nu_{as}(CCO)$	1176	$\delta(CH)_{rock}$	1190	1200 vw	1197 vw
229	$\tau\,(CH_3)$	1038 (d), 1033	ν(CC)	1171	$\delta(OH)_{ip} + \delta(CH_2)_{rock}$			
137	τ (CC)	895, 898 (d)	$\delta\,(CH_2)_{twist} + \delta(CH)_{rock}$	1149	$\delta(C-OH)_{ip} + \delta(CH)_{rock}$	1142	1138	1137,
		891 (d)	$\delta(CH_3)_{rock} + \nu$(CC)	1133	$\delta(CH_2)_{wagg} + \delta(C-OH)_{ip}$			1160 w, br
		704 (d)	$\delta(C-OH)_{op}$	1130	$\nu(CO) + \delta(CH)_{rock}$			
		472, 461 (d)	δ (CCO)	1128	$\delta(CH_2)_{twist} + \delta(CH_3)_{rock}$	1111	1113	1110
		370	$\delta\,(C-OH)_{op}$	1095, 1085, 1080	$\nu(CC) + \nu_{as}(CCO)$	1069 vw	1054vw	1054 vw
		280 (d), 268	δ (CCC)	1038	ν(CC)	1021 vw		1012 vw
		237, 230 (d)	$\tau\,(CH_3)$	995, 991	$\nu(CC) + \delta(CH_3)_{rock}$	991 vw		
		166 (d), 142	τ (CC)	960	$\delta(C-OH)_{op} + \delta(CH_3)_{rock}$	969	945 vw, 965 vw	940−90 vw
		125, 82, 60, 46	intermolecular	928, 915, 896, 894	$\delta\,(CH_2)_{twist} + \delta(CH)_{rock}$	892	882	886, 922 sh
				869, 865	ν(CC)	860 w, sh	854 sh	851 vw
				779 (C2)	$\delta(CH_2)_{rock}$	807 vw		793 sh
				782, 767, 761	$\delta(C-OH)_{op} + \delta(CH_2)_{rock}$	760	759	758
				699	$\delta(C-OH)_{op}$	690 w	640 vw, br	
				504, 489, 478	δ (CCO)	463 (485)	466 (486)	461 (486)
				335, 321, 290	δ (CCC)	327	327	326
					δ (CCC) + $\tau\,(CH_3)$	274 br	250−300 br	288
				255, 238, 235	$\tau\,(CH_3)$	233	224	232
				210, 205, 186, 153	τ (CC)	158	164 w	
				153, 133, 110, 89, 80, 63, 59, 45, 36	intermolecular	99 sh, 73 br	130, 100 sh, 73 br	127, 83 s, 57 s

[a] aCLIMAX fit to 1-propanol DFT data. [b] All frequencies are in cm^{-1}; vs = very strong, s = strong, m = medium, w = weak, vw = very weak, sh = shoulder, br = broad, d = H-donor molecule.

TABLE 5: Experimental Vibrational Frequencies, Assignments of the INS Bands of 1-Butanol in the Solid and Adsorbed (Three 1-Butanol Molecules per Faujasite Supercage, on Average) State (T < 20 K), and Theoretical Vibrational Frequencies of 1-butanol Clusters Calculated by DFT

DFT		DFT		INS[b]	
monomer $M_{TTg'}$	assignment[a]	linear dimer $D_{GTg'GTt}$	assignment[a]	solid	Na−X
1562	$\delta_{as}(CH_3)$	1541, 1530 HB	$\delta_{as}(CH_3) + \delta(CH_2(O))$	1458 br	(1800−1200) 1451
1551	$\delta_{as}(CH_3) + \delta(CH_2(O))$	1524, 1522, 1520, 1516 (d), 1511, 1504 (d)	$\delta_{as}(CH_3) + \delta(CH_2(C))$		
1576 (C^1)	$\delta(CH_2(O))$	1499 (d)	$\delta(CH_2(C))$		
1545	$\delta(CH_2(C))$	1466 (d)	$\delta(OH)_{ip}$		
1468 (C^1), 1466	$\delta(CH_2)_{wagg} + \delta_s(CH_3)$	1463	$\delta(CH_2)_{wagg} + \delta(OH)_{ip}$		
1437, 1410	$\delta(CH_2)_{wagg} + \delta(OH)_{ip}$	1431 (d)	$\delta(CH_2)_{wagg} + \delta_s(CH_3)$	1430 sh	
1365	$\delta(CH_2)_{twist}$	1430	$\delta_s(CH_3)$		
1353	$\delta(CH_2)_{twist} + \delta(OH)_{ip}$	1424 (d)	$\delta(CH_2)_{wagg} + \delta(OH)_{ip} + \delta_s(CH_3)$		
1314	$\delta(CH_2)_{wagg}$	1391	$\delta(CH_2)_{wagg} + \nu(CC)$		
1275	$\delta(OH)_{ip} + \delta(CH_2)_{rock}$	1384 (d), 1354 (d)	$\delta(CH_2)_{wagg} + \delta(CH_2)_{twist}$	1368 br	1378
1179	$\nu(CC, CO) + \delta(CH_3)_{rock}$	1375	$\delta(CH_2)_{wagg} + \delta(OH)_{ip}$		
1137	$\delta(CH_2)_{twist} + \delta(OH)_{ip}$	1333	$\delta(CH_2)_{twist}$		
1119	$\nu_{as}(CCO)$	1314	$\delta(OH)_{ip} + \delta(CH_2)_{wagg} + \delta(CH_2)_{twist}$		
1103, 1038	$\nu(CO) + \nu(CC)$	1291 (d)	$\delta(CH_2)_{twist} + \delta(CH_2)_{wagg}$	1296	1298
973	$\delta(CH_2)_{twist} + \delta(C^1H_2)_{wagg}$	1254	$\delta(OH)_{ip} + \delta(CH_2)_{twist}$	1251	1259 sh
940	$\delta(CH_3)_{rock} + \nu(CC) + \delta(CH_2)_{wagg}$	1244	$\delta(CH_2)_{twist} + \delta(OH)_{ip}$		
825, 759	$\delta(CH_2)_{rock}$	1227 (d), 1163 (d), 1112	$\delta(CH_2)_{twist} + \delta(OH)_{ip} + \delta(CH_3)_{rock}$	1218	1214
454	$\nu(CCO)$	1182	$\delta(CH)_{rock}$		
400	$\delta(CCC)$	1124 (d)	$\delta(OH)_{ip} + \delta(CC) + \delta(CH_3)_{rock}$	1115 w, br	1114
324	$\delta(OH)_{op}$	1093 (d)	$\nu_{as}(CCO)$		
186	$\delta(CCC)$	1087, 1073 (d)	$\nu_{as}(CCC)$		
264	$\tau(CH_3)$	1045	$\nu(CO) + \nu(CC)$	1058 vw, br	1052 vw, 1023 vw
128, 110	$\tau(CC)$	981	$\delta(CH_3)_{rock} + (CH_2)_{wagg} + \delta(CH_2)_{twist}$		
		965, 962 (d)	$\nu(CC) + \delta(CH_2)_{twist}$	966 sh	
		976 (d)	$\delta(CH_3)_{rock} + \nu(CC) + \delta(CH_2)_{wagg}$	948	944
		887 (d), 884	$\nu_s(CCC)$	898 w	889 vw
		816,	$\delta(CH_2)_{rock}$	842, 826 w	839 w
		801 (d), 760	$\delta(CH_2)_{rock} + \delta(CH_3)_{rock}$	798 m	797
		755 (d)	$\delta(CH_2)_{rock} + \delta(OH)_{op}$	736	736
		734 (d)	$\delta(OH)_{op}$	690 w, br	640 vw, br
		490 (d, a)	$\delta(CCC) + \delta(OCC)$	516, 453 w	517, 448
		358 (d)	$\delta(CCC) + \delta(OCC)$	394, 351 w	394, 356
		352	$\delta(OH)_{op} + \delta(CCC)$		
		335	$\delta(OH)_{op}$		
		296, 225, 212	$\delta(CCC) + \tau(CH_3)$	254 m, 192 vw	285, 190
		290 (d)	$\tau(CH_3)$	254	261
			$\delta(OH\cdots O)$	194 vw, sh	190 w
		135, 120, 112	$\tau(CC)$	139 sh	132 br, 156 sh
		101, 69	$\tau((O)CC)$	82 s	73, 99
		46, 34	intermolecular		42

[a] aCLIMAX fit to 1-butanol DFT data. [b] All frequencies are in cm^{-1}; vs = very strong, s = strong, m = medium, w = weak, vw = very weak, sh = shoulder, br = broad, and d = H-donor molecule.

types of interactions between the alkane chains of the alcohol molecules are assumed. This inductive effect of the oxygen atom on neighboring CH_n groupings was also observed for esters.[52]

In addition, the difference for ethanol and 1-propanol might also be due to an enhanced intramolecular van der Waals interaction between the ethanol CH_3 protons and the free electron pairs of the oxygen atom, both being on the same site and closer to each other than for 1-propanol.

Hydrogen Bonding of Functional OH Groups. The absence of the $\delta(OH)_{op}$ vibrations of an unperturbed OH group (located at 290−370 cm^{-1} according to the theoretical calculations and IR and Raman spectra[12,27,34,38]) in the spectra of all solid alcohols indicates that all hydroxyl groups are hydrogen bonded. For solid methanol, the doublets at 650 and 760 cm^{-1} are attributed to the hydrogen-bonded $\delta(OH)_{op}$ vibrations,[27] whereas only a weak, broad band was observed for the other alcohol molecules with a maximum at 715 cm^{-1} for ethanol and 690 cm^{-1} for 1-propanol and 1-butanol.

In contrast to the doublet observed for the $\delta(OH)_{op}$ mode of the ordered structure of solid methanol crystallized in the low-temperature α phase,[16,17] ethanol and the higher alcohols gave

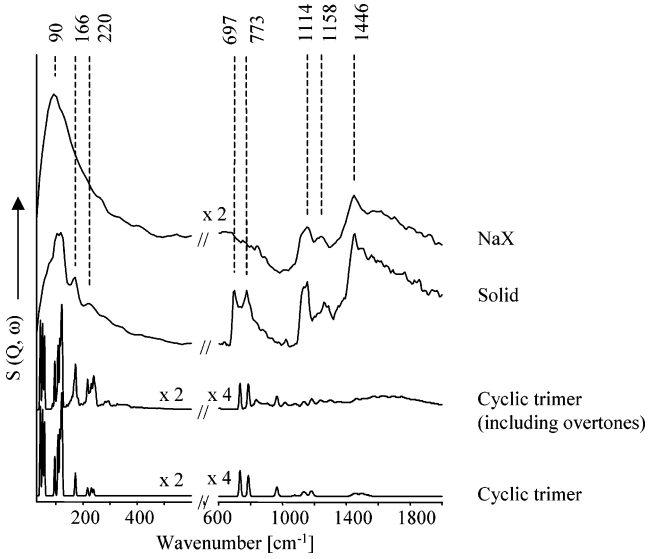

Figure 2. Theoretical vibrational spectra of cyclic methanol trimer cluster and inelastic neutron scattering spectra of methanol adsorbed on Na−X (loading three molecules per supercage, on average) and solid methanol at T < 20 K.

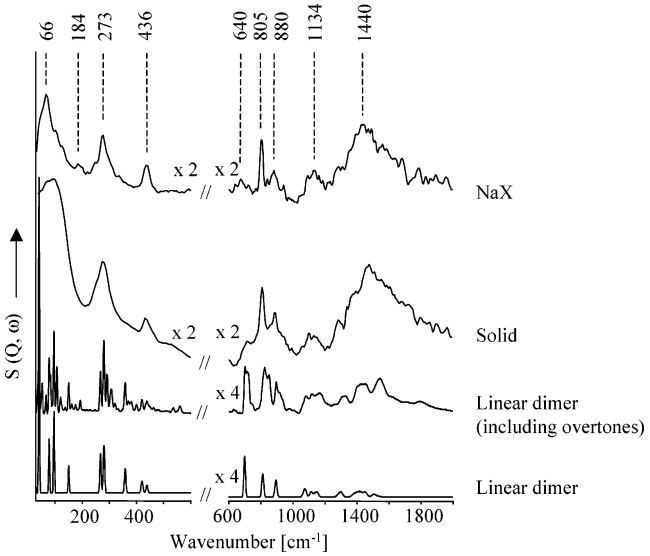

Figure 3. Theoretical vibrational spectra of linear ethanol dimer cluster and inelastic neutron scattering spectra of ethanol adsorbed on Na−X (loading three molecules per supercage, on average) and solid ethanol at $T < 20$ K.

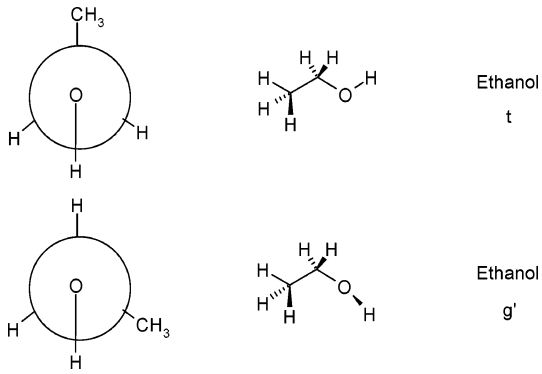

Figure 4. Conformers of ethanol used for DFT calculations

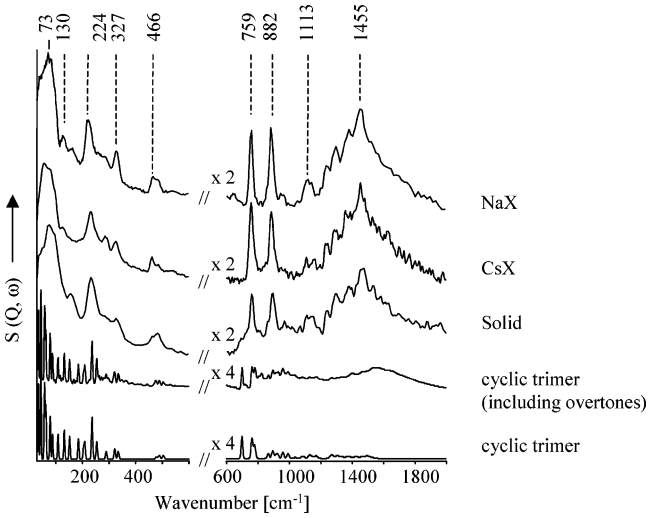

Figure 5. Theoretical vibrational spectra of cyclic 1-propanol trimer cluster and inelastic neutron scattering spectra of 1-propanol adsorbed on Na−X (loading three molecules per supercage, on average) and solid 1-propanol at $T < 20$ K.

strongly broadened peaks for this mode without a defined splitting (Figures 2, 3, 5, and 7). For crystalline methanol, band splitting is obtained because of the presence of two crystallographically independent molecules in the unit cell joined by H bonds.[53,54] For crystalline ethanol, band splitting is conceptually expected because of the presence of four ethanol molecules consisting of two crystallographically independent molecules joined by H bonds in the monoclinic unit cell.[55] The absence indicates that ethanol was probably present in an amorphous state or at much lower cluster size than in the crystalline form. Note that the splitting (with bands at 660 and 580 cm^{-1}) was reported for single crystals of ethanol,[56] but the second band was broadened and of very low intensity. Splitting of several internal modes of the ordered structure of solid ethanol has been also observed, which may be the reason for the broadening of our INS signals. Hydrogen-bonded OH groups in liquid and amorphous ethanol have been attributed to the broad signals at 660 and 690 cm^{-1},[57] respectively, and in liquid 1-propanol, to a band at 670 cm^{-1}.[37]

Longitudinal Acoustic Modes (LAMs). The in-plane deformation vibrations of the C−C−C(O) bond angles and C−C(O) bond stretching vibrations are typically described as longitudinal acoustic modes (LAMs).[51] These are the lowest-frequency molecular vibrations involving the extension of the (hydrocarbon) chain located in the energy region between 0 and 530 cm^{-1}. The number of bands observed increases as the number of CH_2 units in the hydrocarbon chain increases. For linear alcohol and alkanes with n carbon atoms, $n - 2$ LAM modes are expected. When a carboxylate group was substituted for a terminal methyl group in long n-alkanes, the LAM sequences remained remarkably similar to those of the parent chains.[58] For the short-chain alcohols investigated here, the influence of the functional OH group is still dominant. For propane, n-butane, and n-pentane,[47] LAMs were found at 267, 180, and 425, and at 129, 386, and 450 cm^{-1}, respectively. In theoretical calculations for alcohols of the same chain length, the LAMs resulted in higher frequencies of the corresponding vibrations, which can be attributed to the presence of oxygen atoms. For ethanol, the δ(CCO) mode is found at 430 cm^{-1}.[34] For 1-propanol, the bands at 326 and 465 cm^{-1} are assigned to δ(CCO) and δ(CCC) LAM modes, respectively. In the later mode, all CCC bond angles expand or contract in phase. The calculated frequencies of the LAMs of 1-propanol are 335 (Gg + Gt), 321 (Gg + Gt), 290 (Tg) and 504 (Gg + Gt), 489 (Gg), and 478 cm^{-1} (Tg) for the different conformers of the cyclic trimer cluster. The results show clearly that the frequencies depend on the molecule conformation. The first LAM mode was attributed to both trans and gauche conformers, whereas the latter was due to only the trans conformer.

In the spectrum of solid 1-butanol, six INS signals were assigned to LAMs (516, 453, 351, 394, 254, and 192 cm^{-1}), indicating the existence of several conformers (Table 8). In comparison to the band assignment obtained by Ohno et al.[38] on the basis of a detailed conformational study of 1-butanol, the bands at 192, 398, 452, 798, 898, and 948 cm^{-1} can be attributed to the TTt and/or the TTg conformer, whereas the bands at 254, 352, 518, 826, 842, and 966 cm^{-1} are due to the TGx conformers, where x indicates a t, g, or g′ conformation about the C−O axis. The first three signals of each series are LAMs, whereas the latter ones are mainly assigned to rocking vibrations. In the solid state of 1-propanol, TTt and/or TTg forms were found to exist, whereas in the glassy state and liquid state, the TGx form was also found on the basis of the calculated results.[38] Thus, we may conclude that under the conditions studied solid 1-butanol is present in an amorphous phase, whereas for 1-propanol, the band at 485 cm^{-1} may indicate an additional LAM frequency, which indicates the presence the Gg conformer. In addition, the absence of the splitting of the δ(COH) mode tentatively points to the formation of an

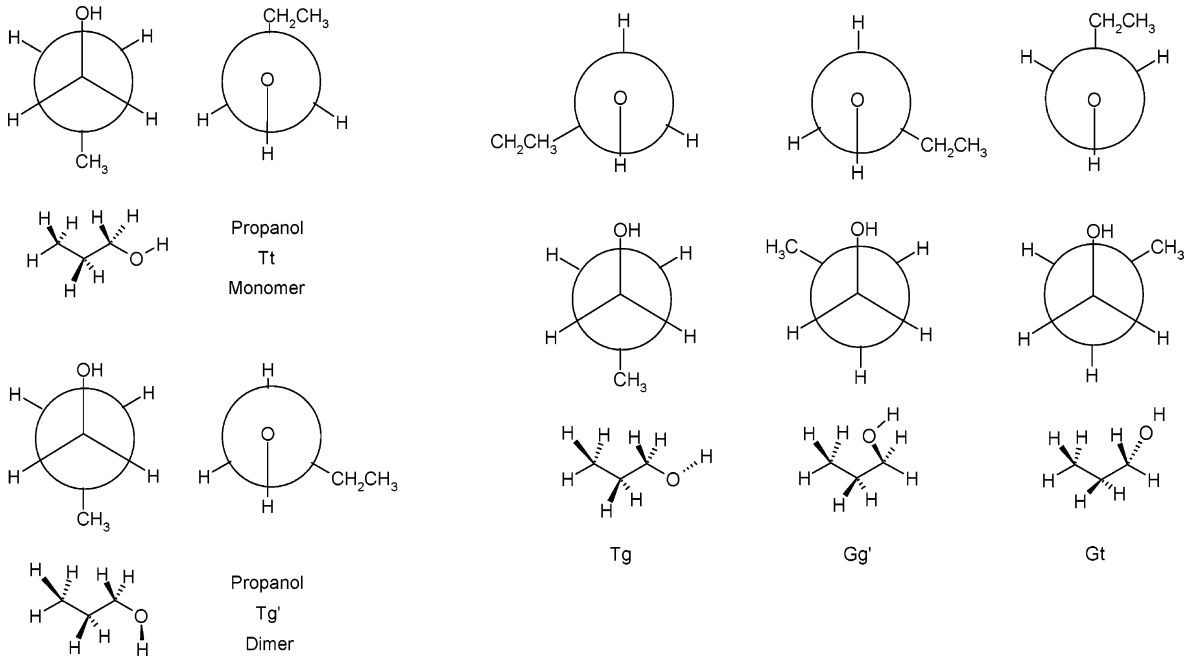

Figure 6. Conformers of 1-propanol used for DFT calculations

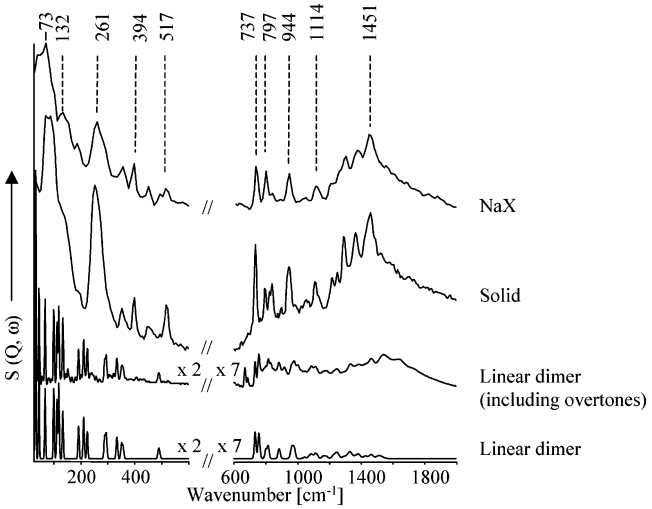

Figure 7. Theoretical vibrational spectra of linear 1-butanol dimer cluster and inelastic neutron scattering spectra of 1-butanol adsorbed on Na−X (loading three molecules per supercage, on average) and solid 1-butanol at $T < 20$ K.

amorphous solid state for all C_2-C_4 alcohols[27] formed under the conditions studied. Note that the band at 485 cm^{-1} may also be assigned to the first overtone mode of the methyl torsion vibration at 233 cm^{-1}.

Alcohols Adsorbed on Na−X. *OH Stretching and Deformation Vibrational Modes.* All hydroxyl groups of the investigated alcohols, adsorbed on Na−X, appear to be hydrogen bonded as indicated by the absence of the $\delta(OH)_{op}$ mode of freely vibrating OH groups in the INS spectra, which resembled the INS of the solid alcohols. The weak and broad feature, observed in all INS spectra of the adsorbed alcohols between 570 and 750 cm^{-1}, is assigned to the hydrogen-bonded $\delta(OH)_{op}$ mode. With increasing chain length, the maximum is shifted slightly to lower wavenumbers (675 cm^{-1} for ethanol and 640 cm^{-1} for 1-propanol and 1-butanol), but it is very weak compared to the hydrocarbon modes. Note also that in the solid materials this band was broadened and of low intensity for the C_2-C_4 alcohols, which is attributed to an amorphous state or polycrystalline (very small crystal sizes) state compared to the crystalline phase found for methanol as discussed above. This leads to the conclusion that self-association of the C_2-C_4 alcohols in the faujasite cage forming crystalline clusters does not take place and that the hydrogen-bond strength is lower than in the solid. Because of the broadening, it is also possible that more than one alcohol adsorption structure exists.

In the infrared spectra (Figure 9), the stretching mode of the alcohol OH groups is very intense and clearly separated from the stretching vibrations of the CH groups. Compared to the vibrational mode in the gas phase, the ν(OH) stretching mode was strongly broadened and shifted to lower wavenumbers, confirming the hydrogen-bond formation proposed from the INS data. Identical to the adsorption of methanol,[27] a shoulder at higher frequencies was observed for the C_2-C_4 alcohols, indicating the formation of at least two sorption structures. In Figure 13, the ν(OH) frequencies of the various alcohols, adsorbed on Na^+-, K^+-, and Rb^+-exchanged X zeolites, are related to the electronegativity of the countercation. The frequency shift of the ν(OH) stretching mode showed a strong dependence on the basicity of the zeolite and only a subtle dependence on the chain length of the alcohol molecules. With increasing framework polarity (from Na−X to Rb−X), enhanced hydrogen bonding between the sorbates and the zeolite oxygen atoms is observed, which is reflected by the decreasing ν(OH) frequency. The OH stretching vibration signal showed the highest frequency for alcohols adsorbed on the least basic sample, Na−X, (~3350 cm^{-1}) and decreased to lower wavenumbers for the more basic K−X (3270 cm^{-1}) and Rb−X (~3250 cm^{-1}) samples.

By exchanging countercations of lower Lewis acidity into the zeolite structure, for example, Rb^+, a higher negative charge is located on the zeolite oxygen atom,[27] thus stronger basic materials are obtained. For alkali cation-exchanged ZSM-5 materials having a relatively apolar zeolite framework, the extent of the downward shift of the OH group was found to decrease proportionally with the increasing radius of the countercation, indicating the dominating interaction between the alkali cation and the oxygen atom of the alcohol.[59] Note that the direct interaction between the lone-pair electron donor function of methanol via the oxygen atom of the hydroxyl group and the

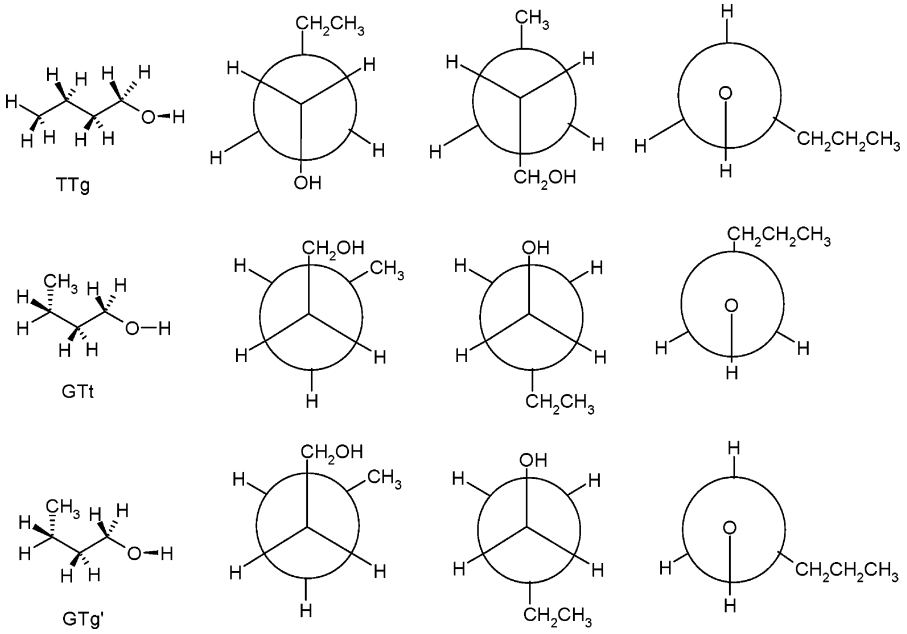

Figure 8. Conformers of 1-butanol used for DFT calculations.

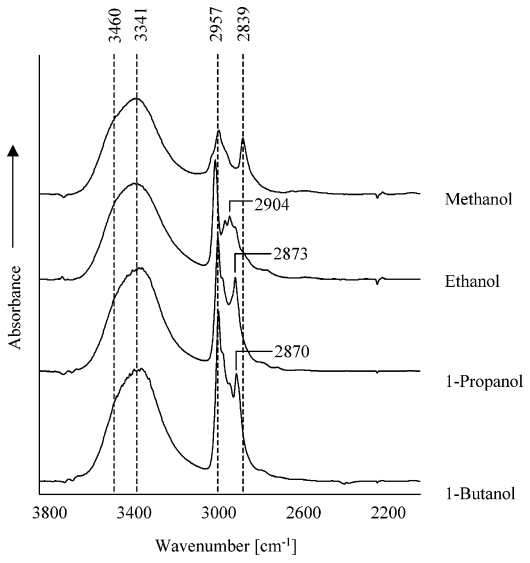

Figure 9. Difference infrared spectra of C_1-C_4 alcohols adsorbed on Na−X ($T = 308$ K, $p = 1 \times 10^{-3}$ mbar).

electron pair acceptor function of the zeolite (the alkali-metal cation) was identified by DFT calculations as the most important energetic contribution to sorption.[60]

For C_1-C_4 alcohols adsorbed on Na−X, the perturbation of the alcohol OH group increased only slightly with increasing hydrocarbon chain length. This increase in the shift may be explained by a larger positive inductive effect of CH_2R groups with increasing *n*-alkyl chain length, thus leading to slightly enhanced hydrogen-bond formation of the alcohol OH proton.[61] For 1-propanol and 1-butanol, similar wavenumbers were observed, which is typical for the markedly decaying inductive effect.[48] The alcohol oxygen atom possesses increasing electron density with increasing *n*-alkyl chain length, but the influence of each added carbon atom diminishes with the spatial separation of the carbon atom to the hydroxyl group. Note that for K−X and Rb−X the ν(OH) shift of adsorbed alcohol first decreases but then increases with increasing alcohol chain length. These higher ν(OH) frequency values obtained for 1-butanol, adsorbed on K−X, and 1-propanol and 1-butanol, adsorbed on Rb−X, can be attributed to increasing steric hindrance with the molecule size. Also, increasing hydrogen-bond formation between the CH groups and the stronger polar framework may influence the inductive effect of the hydrocarbon chain and decrease the electron density on the alcohol O atom and thus strengthen the alcohol OH bond.

The low resolution of the INS signals makes it difficult to assign frequencies for the $\delta(OH)_{ip}$ deformation bending vibrational bands of the alcohol hydroxyl groups, which are additionally strongly broadened and overlapped by the $\delta(CH)_{ip}$ bending modes of the alcohol methyl and methylene groups. From the calculation, a combination of the δ(OH) bending mode with the $\varpi(CH_2)$ band is also found; thus, the decrease of the modes at 1423 sh, 1418, 1410, and 1410 cm^{-1} cannot be related to a decreasing hydrogen-bonding strength of the alcohol OH group. However, the $\delta(OH)_{ip}$ vibrations are still found at higher wavenumbers for all adsorbed alcohols as compared to those for the monomers (e.g., for ethanol in the gas phase, 1241 cm^{-1} [62]), supporting hydrogen bonding of the alcohol hydroxyl groups. Evidence of alcohol decomposition into surface methoxy groups or formates (to be indicated by bands at 1635 and 1610 cm^{-1}) was not observed under the adsorption conditions used.

CH Vibrational Modes. The INS spectra of adsorbed alcohol molecules exhibit typical vibrational CH bands similar to those found for the solid phase. Most bands are broadened, indicating a lack of long-range order and multiple states of alcohols adsorbed on the zeolite, possibly arising from a low sorbate density. This might enable high flexibility of the alkane chains in the supercage, but an interaction of the molecules via hydrogen bonding of the hydrocarbon chain to the zeolite oxygen atom or other sorbate molecules is also conceivable.

For ethanol adsorbed on Na−X, the methyl torsional mode (276 cm^{-1}) and the LAM (436 cm^{-1}) are shifted to higher wavenumbers, whereas the torsional mode of adsorbed 1-propanol was found at slightly lower frequencies (224 cm^{-1}) compared to their solid counterparts (233 cm^{-1}). Because of the coordination of the alcohol oxygen atom to the countercation, the electron density decreases, and the electron-withdrawing effect of the alcohol OH group on the alkane chain increases, leading to a further-enhanced contraction and elongation of the $C^{\alpha}-C^{\beta}$ and $C^{\beta}-C^{\gamma}$ bonds, respectively, as already seen for the

TABLE 6: Vibrational IR Frequencies of Linear C_1-C_4 Alcohols Adsorbed on Na−X ($T = 308$ K, $p = 1 \times 10^{-3}$ mbar)

methanol				ethanol				
assignment[a]	gas phase[83]	liquid[44]	ads on Na−X	assignment[a]	gas phase[46,70]	liquid[47]	ads on silica[86]	ads on Na−X
ν(OH)	3682 s	3337 s, br	3460 sh, 3341 s, br	ν(OH)	3676	3330[87,88]	3326	3459 sh, 3335 vs br
ν(CH_3) as	2999, 2970	2934	2980 sh, 2957 br	ν_{as}(CH_3)	2989	2975	2982	2970 vs
2 × δ(CH_3)	2920		2917	ν_{as}(CH_2)	2948			2955 sh
ν(CH_3) s	2844	2822	2839 br	ν_s(CH_3)	2943	2927	2932	2923 m
δ_{as}(CH_3)	1477, 1465, 1454	1475, 1453	1476, 1451	ν_s(CH_2)	2900	2886	2908, 2880	2904 m, 2874 m sh
				2xδ($COH)_{ip}$	2890			2838 w sh
δ(OH), δ_s(CH_3)		1420 br	1423 sh, 1400 br	δ(CH_2)	1490	1484	1496, 1484	1478 w
δ(OH)	1340			δ_{as}(CH_3)	1452	1455, 1447	1452	1452 m
				$\delta(COH)_{ip} + \omega(CH_2)$		1420		1418 m b
				ρ(CH_2)			1400	
				δ_s(CH_3), ω(CH_2)	1394	1380	1378	1386 sh, 1361
				$\delta(COH)_{ip} + \omega(CH_2)$		1331		1327

1-propanol					1-butanol			
assignment[a]	gas phase[33]	liquid[72]	ads on Na−X	ads on Rb−X	assignment[a]	matrix [31] (15 K)	liquid[31]	ads on Na−X
ν(OH) monomer	3687				ν(OH) monomer	3670 s, 3663 m br, 3647 w		
ν(OH) polymer		3356	3459 sh, 3329 vs b	3252 vs b	ν(OH) polymer	3517 dimer 3466 vw br, 3434 vw br	3336 vs, br	3460 sh, 3327 vs br
ν_{as}(CH_3)	2978	2967	2958, 2953 sh	2956				
ν_{as}(CH_2)	2946, 2929				ν_{as}(CH_3)	2974 vs, 2970 vs sh	2961 vs	2955 s
ν_s(CH_3)		2933	2937	2932	ν_{as}(CH_2)	2943		
ν_s(CH_2)	2892	2874	2875 s	2867 s	ν_s(CH_3)	2932 s sh	2935 vs	2933 m sh
δ(CH_2(O))			1474 w		ν_s(CH_2)	2910 m, 2903m, 2885 s, 2873 m sh		2899 m sh, 2870 s
δ_{as}(CH_3), δ(CH_2)	1464	1464	1463 w sh, 1459 m	1459 m b	2×$\delta(COH)_{ip}$ δ(CH_2)			2854 sh
δ(CH_2(C))			1436 sh	1442 w sh	δ(CH_2(O))	1485 vw, 1480 vw, 1470 s		1478 sh
$\delta(COH)_{ip} + \omega(CH_2)$			1412 b					
ω(CH_2)	1393, 1300	1300	1395		δ_s(CH_3)	1470 s, 1466 vs, 1460 s	1466 s, 1460 s sh	1462 m
δ_s(CH_3)	1393		1391	1390				
t(CH_2)	1276				δ_s(CH_3), δ(CH_2(C))	1457 vw, 1454 vw		
$\delta(COH)_{ip}$	1218	1381	1343	1349	δ(CH_2(C))	1440 w, 1437 vw	1434	
					$\delta(COH)_{ip} + \omega(CH_2)$	1434 vw, 1410 vw, 1395 vw br	1425 w sh	1410 br
					$\delta(COH)_{ip} + \delta_s(CH_3)$	1383 m		
					δ_s(CH_3)	1382 m	1379 s	1387
					ω(CH_2)	1348 vw, 1342 vw	1369 w sh	1342 w
					$\delta(COH)_{ip}$		1339 m	
					ω(CH_2)	1309 vw	1328 w sh	

[a] All frequencies are in cm^{-1}; vs = very strong, s = strong, m = medium, w = weak, vw = very weak, sh = shoulder, br = broad, and d = H-donor molecule.

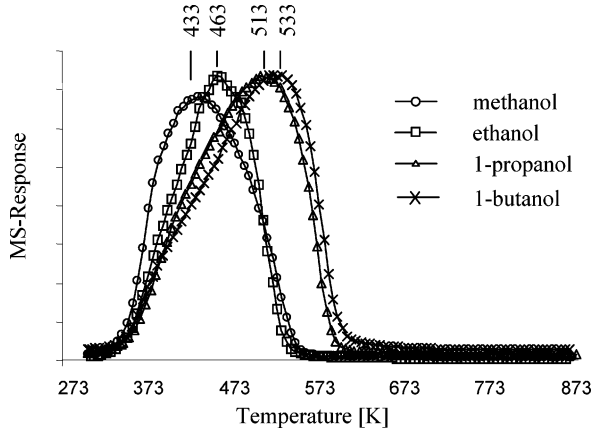

Figure 10. Temperature-programmed desorption of C_1-C_4 alcohols adsorbed on K−X.

solid materials and is in line with a more hindered torsional vibration for adsorbed ethanol and a less hindered one for 1-propanol. For 1-propanol adsorbed on Cs−X, the torsion vibration (232 cm^{-1}) was found at a similar value to that for the solid alcohol. This can be explained by the coordination of the alcohol oxygen atom to the Cs countercation, which is of lower strength than on Na−X because of the lower Lewis acidity of the Cs cation. The electron density of the alcohol oxygen atom, and hence the inductive effect of the alcohol OH group, will not change significantly, leading to an unchanged methyl torsion around the $C^{\beta}-C^{\gamma}$ bond.

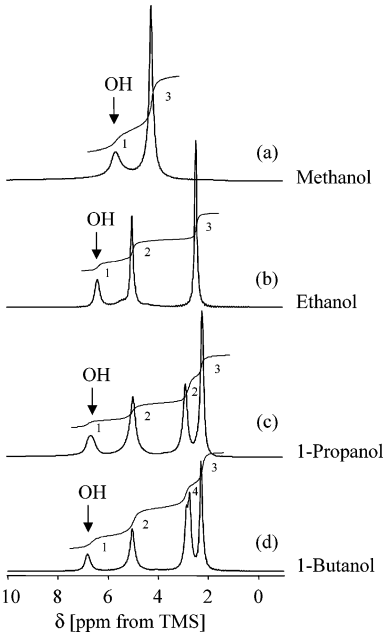

Figure 11. ^1H MAS NMR spectra of C_1-C_4 alcohols adsorbed on Na−X.

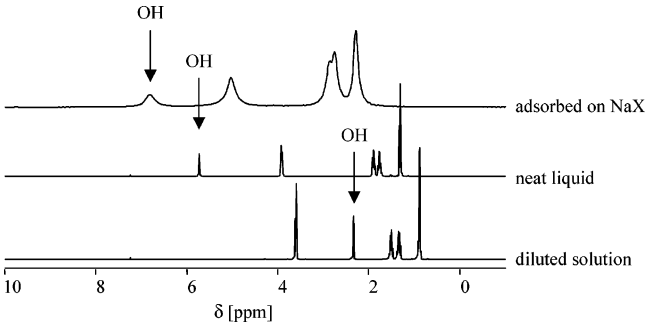

Figure 12. ^{1}H MAS NMR spectra of 1-butanol diluted in CCl_3D (0.312 mmol), as neat liquid, and adsorbed on Na−X.

TABLE 7: ^{1}H Chemical Shifts of Alcohols and Alcohols Adsorbed on Zeolites from TMS

sorbate/sorbent	OH	$-CH_2-$	$-CH_2-$	$-CH_2-$	$-CH_3$
liquid NMR					
methanol (CCl_3D)	2.01				3.44
ethanol (CCl_3D)	2.41	3.67			1.20
1-propanol (CCl_3D)	2.45	3.55	1.54		0.89
1-butanol (CCl_3D)	2.34	3.60	1.51	1.34	0.89
methanol (neat liq)	5.68				4.09
butanol (neat liq)	5.73	3.92	1.90	1.77	1.32
solid-state NMR					
methanol on Na−X	5.66				4.24
ethanol on Na−X	6.38	5.01			2.46
1-propanol on Na−X	6.65	4.96	2.88		2.21
1-butanol on Na−X	6.82	5.04	2.87	2.76	2.30
CD_3OH on Na−Y [55]	4.7				
CD_3OH on Na−ZSM-5 [55]	3.6				
methanol on Na−ZSM-5 [55]	∼2.9 sh				4.1
methanol on H−ZSM-5 [55]	9.4				4.1

For the ν(CH) stretching vibrational bands, a similar trend, as already described for the ν(OH) stretching vibration, was observed in the infrared spectra. In agreement with the results obtained from Rep et al.[11] the bands of adsorbed methanol, assigned to the asymmetric and symmetric $\nu(CH_3)$ stretching modes, were found to be broadened and shifted to lower frequency values compared to that of the gas-phase spectrum (2989 cm^{-1} [62]). This observation is explained by a multitude of states due to hydrogen-bond formation between the methyl group and the negatively charged zeolite oxygen atom. Similar to methanol adsorption, the symmetric and asymmetric $\nu(CH_3)$ stretching vibrational bands of adsorbed ethanol appear at lower wavenumbers relative to that of the gaseous alcohol. The wavenumbers are not only higher compared to that of methanol but also related to hydrogen-bond formation. Note that with increasing chain length the signal of the methylene groups increased in intensity and overlapped with the asymmetric $\nu(CH_3)$ signal.

Assuming that the inductive effect of the alcohol O atom mainly influences the α-CH_2 group, the methyl stretching vibration is expected to occur at similar frequencies for 1-propanol and 1-butanol as that found for ethanol (minor differences may be due to the inductive effect of the hydrocarbon chain as found by INS), whereas the shift of the band maximum at 2970 cm^{-1} (for ethanol) to 2958 and 2955 cm^{-1} (for 1-propanol and 1-butanol, respectively) is attributed to the increasing contribution of the $\nu(CH_2)$ vibration to the band intensity. The increased frequency of the band assigned to the $\nu_{as}(CH_2)$ vibration of adsorbed ethanol (shoulder at 2955 cm^{-1}) compared to the gas-phase value (2948 cm^{-1}) is explained by a decrease in the electron density of the alkyl group due to the coordination of the ethanol oxygen atom to the cation, which further leads to an increase in the CH stretching frequency.[63] It may also indicate that the methylene group is not hydrogen bonded to the framework.

For the adsorption of 1-propanol on nonpolar Rb−ZSM-5 (Figure 14), the interactions between the lattice oxygen and hydrocarbon chain are minimal compared to those of the aluminum-rich X zeolites. The asymmetric $\nu(CH_3)$ vibrational band at 2967 cm^{-1} is located at the same wavenumber as that for liquid 1-propanol,[64] whereas the symmetric $\nu(CH_2)$ appears at higher frequencies (2882 cm^{-1} as compared to 2975 cm^{-1}). This shift of the symmetric stretching vibration is attributed again to minor strengthening of the C−H bonds in response to the elongation of the C−O bond as a result of the interactions of the sorbate molecule with the metal cation.[65] After the adsorption of 1-propanol on Na−X, the symmetric $\nu(CH_2)$ band is shifted in the opposite direction to 2875 cm^{-1}, indicating lateral interaction of the hydrocarbon chain either to the pore wall or between adsorbed molecules as in the liquid state. After changing the countercation Na^+ to Cs^+ (increasing the framework polarity), the ν(CH) bands are the wavenumbers observed, suggesting that the CH groups interact with the pore walls.

The presence of two symmetric $\nu(CH_2)$ stretching bands at 2904 and 2880 cm^{-1} for ethanol and 2899 and 2870 cm^{-1} for 1-butanol suggests the presence of different adsorption structures. The weak band at 3740 cm^{-1} appears to be caused by weakly adsorbed sorbate molecules because it is not present after evacuation of the sample at room temperature.

Strength and Mode of Interaction of the Alcohols. The ^{1}H MAS NMR resonance of protons of the $^{\alpha}$CH group of alcohols adsorbed on Na−X is higher compared to that of alcohols that are highly diluted in CCl_3D, where hydrogen bonding is nearly absent (Table 7). This indicates a stronger deshielding of the protons of adsorbed alcohols, that is, a lower electron density on the alcohol O atom. This leads to an increased inductive effect on the neighboring CH_2 group and is related to the coordination of the alcohol molecules via their oxygen atom to the countercation Na^+. Similarly, the CH_3 resonance was shifted downfield to 4.1 ppm when methanol was adsorbed on H−ZSM-5, [75] forming strong hydrogen bonds to the Brønsted acidic OH groups, or on zeolite Na−ZSM-5 [66] interacting with Na^+ via the methanol oxygens.

The hydroxyl resonance observed for 1-butanol adsorbed on aluminum-rich Na−X (Si/Al = 1.2) was found at much higher values (5.7 ppm) than that for diluted 1-butanol (1.5 ppm) (Figure 12). The observed downfield shift of the OH resonance in the sequence alcohol/CCl_3D < neat alcohol < alcohol on Na−X indicates increasing hydrogen-bonding interactions of the protons. Hydrogen bonding is known to cause large downfield chemical shifts for alcohols because the protons are deshielded by the electrostatic polarization of the OH bond. Note that the deshielding of the OH proton is more enhanced on Na−X than on Na−ZSM-5 (Si/Al = 30; shoulder at 2.9 ppm[66]) and on Na−Y (4.7 ppm; Si/Al = 2.5), indicating stronger hydrogen bonding. Thus, the downfield shift of the OH resonance relative to methanol in CCl_3D is related to the coordination of the O atom to Na^+ and the hydrogen bonding of the proton with the zeolite lattice. The increasing shift in the sequence Na−ZSM5 < Na−Y< Na−X is attributed to an increasingly stronger hydrogen bonding to the more polar zeolite pore wall and additional sorbate−sorbate interactions. It is interesting that the largest shift has been reported for methanol adsorbed on H−ZSM-5, forming strong hydrogen bonds of the alcohol O to the Brønsted acid OH groups of the zeolite.

TABLE 8: LAM Frequencies of the Different 1-Butanol Conformers

1-butanol	calculated[31]							Raman[31] liquid state 295 K	Raman[31] solid state 80 K	INS solid state 20 K		INS Na−X 20 K	
assignment[a]	TTt	TTg	TGt	TGg	TGg′	GTt	GGt		(IR, 295K)	TTt, TTg	TGx	TTt, TTg	TGx
δ(CCO), δ(CCC)			508	518	512		509	516	(515)		516		516
δ(CCC), δ(CCO)						488		488	470 (490)				
δ(CCO), δ(CCC)	436	439						454	445 (452)	453		449	449
δ(CCC)	399	394					392	399	403	394		394	394
δ(CCO), δ(CCC)			343	340	339	344		355			351		356
δ(CCC)			265	269	259	274	266	275	262		254		285
δ(CCC), δ(CCO)	189	186							195	192		195	195

[a] All frequencies are in cm^{-1}; δ = deformation, T, t = trans, and G, g = gauche.

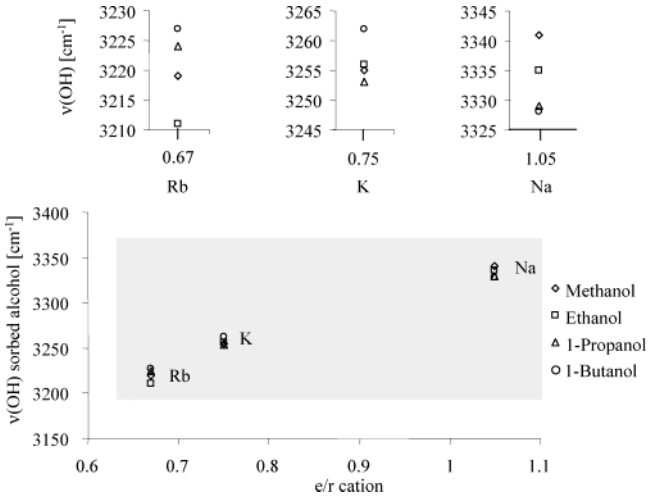

Figure 13. Change of the absorption maximum of the ν(OH) of the sorbed alcohol (T_{ads} = 308 K; $p_{ROH} = 1 \times 10^{-3}$ mbar) as a function of the electronegativity of the cation [$^e/_r$].

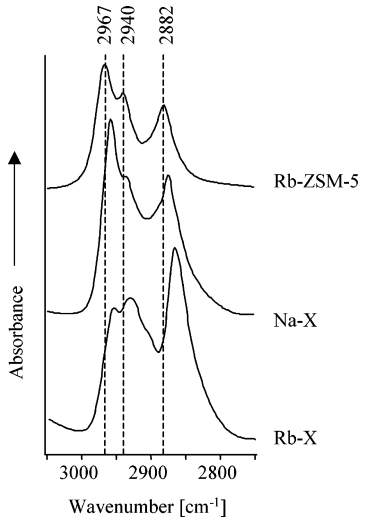

Figure 14. Difference infrared spectra of 1-propanol adsorbed on Rb−ZSM-5, Na−X, and Rb−X (T = 308 K, $p = 1 \times 10^{-3}$ mbar) in the range of 3050−2750 cm^{-1} of ν(CH) stretching vibrational bands.

The continuous increase of the chemical shift of the OH resonance of adsorbed alcohols toward higher frequencies indicates an increasing deshielding of the alcohol OH protons with increasing chain length. This is in line with the frequency shift of the alcohol ν(OH) band observed by infrared spectroscopy (Figure 13). The larger electron density at the alcohol O atom of longer *n*-alcohols leads to stronger hydrogen bonds between the sorbate OH proton, the zeolite O atom, and the neighboring alcohol.

The CH_2/CH_3 resonances of all alcohols were located at higher fields with increasing distance from the oxygen atom. This is in line with the decreasing inductive effect of the electronegative oxygen atom on the CH groups and was also seen for the alcohols in CCl_3D. However, for ROH/Na−X, the resonances were still downfield shifted, which is difficult to relate to the coordination of the alcohol to Na^+. The CH_2 protons resonate at a similar chemical shift, indicating comparable interactions of the hydrocarbon chain independent of the chain length. The higher chemical shift observed as compared to that of unperturbed alcohols (dissolved in CCl_3D) was constant and about 1.3−1.4 ppm. This indicates a comparable deshielding of all CH_2 protons and suggests hydrogen-bond formation of the alkyl protons to the zeolite framework. The thermal desorption of C_1-C_4 alcohols adsorbed on K−X zeolites (Figure 10) shows that the temperature of the desorption maximum increased linearly with increasing chain length (for C_1 to C_4 *n*-alcohols adsorbed on K−X with temperature increase from 433 to 533 K). This is in line with the increase of the heat of adsorption with the number of carbon atoms in the sorbate molecules reported for adsorption on Na−X in ref 67. Because of the only subtle variations in the perturbations of the OH stretching vibrations in this series, the stronger interaction effects are attributed to an increasing contribution of the van der Waals-type interactions between the hydrocarbon chain and the zeolite pore.

On the basis of the ν(OH) frequency shift obtained by IR spectroscopy, the presence of two adsorption structures was suggested.[27] The absence of a more complex OH signal in ^1H MAS NMR suggests that these structures exchange relatively quickly on the time scale of the NMR experiment. However, it should be noted that the signals are broadened and asymmetric.

Adsorption Structures. From the results discussed above, similar sorption structures for short-chain alcohols are deduced. The proposed structure for 1-propanol is shown in Figure 15a. At the low sorbate loading used in this study, a maximum ratio of one sorbate molecule per cation located in the supercage is assumed. Thus, sorbate clustering at a single cation is excluded. 1-Propanol and all other alcohols studied are molecularly sorbed and interact with the countercations via electron donation from the oxygen atom in the alcohol to the alkali metal cation. This mode of adsorption corresponds to the alcohol acting as a base and contributes the most to the binding energy. The strength of this type of bonding depends primarily on the Lewis acidity of the metal cation. The more pronounced downward shift of the ν(OH) stretching vibrational frequency with decreasing Lewis acidity of the metal cation suggests that another type of interaction is simultaneously present that must follow the opposite trend to the coordination of the alcohol to the cation. This interaction is attributed to hydrogen-bond formation

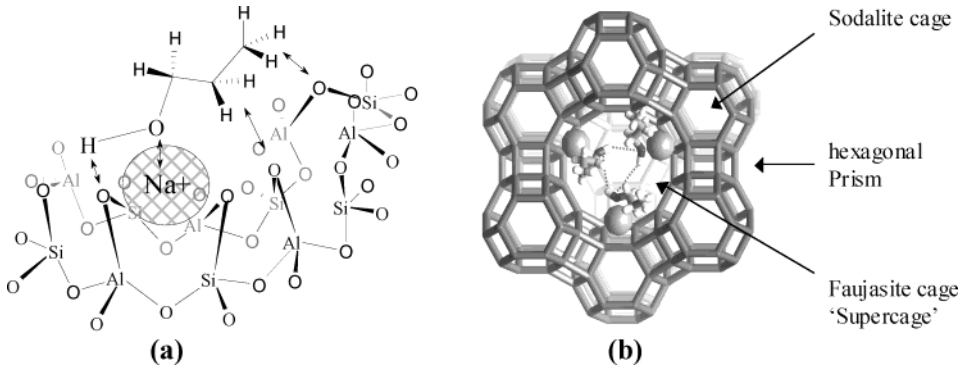

Figure 15. Schematic adsorption structure of 1-propanol adsorbed at SIII on Na−X: (a) single molecule and (b) ringlike structure in supercage window.

between the alcohol OH proton and the negatively charged zeolite oxygen atoms. It increases in strength with increasing framework polarity. The asymmetric shape of the ν(OH) stretching bands and the broadened $\delta(OH)_{op}$ bands suggest a further adsorption structure with a hydrogen-bond interaction between sorbate molecules adsorbed at neighboring cations most likely leading to ringlike sorbate clusters in the faujasite cage (Figure 15b).

The types of interaction are largely independent of the chain length because the frequency shifts in the infrared spectra and the chemical shifts of the OH resonances of adsorbed C_1-C_4 alcohols show only marginal differences for a given zeolite. The differences observed may be attributed to an optimization of the sorption structure with increasing steric hindrance of the larger alcohols, leading to slightly enhanced hydrogen-bond strength. The increasing inductive effect of the hydrocarbon chain on the OH group may also contribute to the stronger interaction. Hydrogen-bond formation between the sorbate hydrocarbon chain and the polar zeolite framework suggests that the hydrocarbon chain of light alcohols is in close contact with the zeolite wall at low loadings.

Conclusions

The hydroxyl groups of the alcohol molecules are completely hydrogen bonded in the adsorbed state similar to the situation in the solid material. During rapid cooling to below 20 K, the solid C_1-C_4 alcohol molecules formed either an amorphous phase or crystals of very small size.

For each of the alkali metal-exchanged zeolites X samples, similar sorption structures exist for all C_1-C_4 *n*-alcohols. The energetic contributions can be separated into strong specific and weaker nonspecific interactions of the (monomeric) alcohol molecules with the cations and the zeolite framework. For the alkali metal cation-exchanged zeolites, the linear alcohol molecules interact primarily via the lone electron pair of the alcohol oxygen with the alkali metal cation (strong specific interactions). Additionally, weaker nonspecific interactions via the hydrogen atoms of the OH groups with the lattice oxygen atoms of the zeolite exist. A second adsorption complex is formed that includes strong hydrogen-bond formation to neighboring adsorbed alcohol molecules.

The extent of the formation of H bonds between the zeolite oxygen atom and the sorbate hydroxyl and methyl groups depends on the framework polarity. Therefore, the strength of the interaction between the alcohol molecules adsorbed and the alkali-exchanged zeolite X is dominated by the properties of the alkai metal cations, which determine the negative charge on the zeolite oxygen atom. Consequently, for the material with the highest basicity (i.e., Rb−X), the strongest interaction between the alcohol molecules and the zeolite was observed.

The different sorption structures of the series of alcohol molecules in particular alkali-exchanged zeolite X samples are attributed to the increasing steric hindrance of the hydrocarbon chain of the larger alcohol molecules and to the increasing inductive effect of the hydrocarbon chain on the OH group, both leading to enhanced hydrogen-bond strength. The formation of hydrogen bonds between the sorbate hydrocarbon chain and the polar zeolite framework indicates close contact between the hydrocarbon chain of light alcohols and the zeolite wall at low loadings.

Acknowledgment. We thank the Deutsche Forschungsgemeinschaft (DFG) within the Sonderforschungsbereich SFB 338: Adsorption an Festkörperoberflächen: Mikroskopische Analyse von Zuständen und Prozessen Teilprojekt B9 as well as ISIS, Rutherford Appleton Laboratory, U.K., for kindly granted measuring time to record the INS spectra.

References and Notes

(1) Barthomeuf, D. *J. Phys. Chem.* **1984**, *88*, 42.
(2) Rossi, F. P.; Busca, G.; Lorenzelli, V.; Lion, M.; Lavalley, J. C. *J. Catal.* **1988**, *109*, 378.
(3) Huang, M.; Kaliguine, S.; Muscas, M.; Aurous, A. *J. Catal.* **1995**, *157*, 266.
(4) Huang, M.; Adnot, A.; Kaliaguine, S. *J. Catal.* **1992**, *137*, 322.
(5) Tanabe, K. *Appl. Catal.* **1994**, *113*, 147.
(6) Tanabe, K.; Hölderich, W. F. *Appl. Catal., A* **1999**, *181*, 399.
(7) Ono, Y. Stud. *Surf. Sci. Catal.* **1980**, *5*, 19.
(8) Yashima, T.; Sato, K.; Hara, N. *J. Catal.* **1972**, *26*, 303.
(9) Yashima, T.; Suzuki, H.; Hara, N. *J. Catal.* **1974**, *33*, 486.
(10) Sidorenko, Y. N.; Galich, P. N.; Gutyrya, V. S.; Ilin, Neimark, Y. G. I. E. *Dokl. Akad. Nauk. SSSR* **1967**, *173*, 132.
(11) Rep, M.; Palomares, A. E.; Eder-Mirth, G.; van Ommen, J. G.; Rösch, N.; Lercher, J. A. *J. Phys. Chem. B* **2000**, *104*, 8624.
(12) Matsumura, Y.; Hashimoto, K.; Yoshida, S. *J. Catal.* **1989**, *117*, 135.
(13) Bonzalez, D.; Cerdeirina, C. A.; Rmani, L.; Carballo, E. *J. Phys. Chem. B* **2000**, *102*, 11275.
(14) Kay, B. D.; Castleman, A. W. *J. Phys. Chem.* **1985**, *89*, 4867.
(15) Provencal, R. A.; Paul, J. B.; Roth, K.; Chapo, C.; Casaes, R. N.; Saykally, R. J.; Tschumper, G. S.; Schaefer, H. F. *J. Chem. Phys.* **1999**, *110*, 4258.
(16) Torrie, H. B.; Weng, S. X. *Mol. Phys.* **1989**, *67*, 575.
(17) Parkes, G. S. *J. Am. Chem. Soc.* **1925**, *47*, 338.
(18) Wertz, D. L.; Kruh, R. K. *J. Chem. Phys.* **1967**, *47*, 388.
(19) Narten, A. H.; Habenschuss, A. *J. Chem. Phys.* **1984**, *80*, 3387.
(20) Montague, D. G.; Gibson, I. P.; Dore, J. C. *Mol. Phys.* **1982**, *47*, 1405.
(21) Hudson, B. S. *J. Phys. Chem. A* **2001**, *105*, 3949.
(22) Fletcher, A. N. *J. Phys. Chem.* **1972**, *76*, 2562.
(23) Ibbilson, D. A.; Moore, L. F. *J. Chem. Soc. B* **1967**, 76.
(24) Ibbilson, D. A.; Moore, L. F. *J. Chem. Soc. B* **1967**, 80.
(25) Fletcher, A. N.; Heller, C. A. *J. Phys. Chem.* **1967**, *71*, 3742.
(26) www.isis.rl.ac.uk.

(27) Schenkel, R.; Jentys, A.; Lercher, J. A.; Parker, S. F. *J. Phys. Chem. B* **2004** *108*, 7902.
(28) Frisch, M. J.; Trucks, G. W.; Schlegel, H. B.; Scuseria, G. E.; Robb, M. A.; Cheeseman, J. R.; Zakrzewski, V. G.; Montgomery, J. A., Jr.; Stratmann, R. E.; Burant, J. C.; Dapprich, S.; Millam, J. M.; Daniels, A. D.; Kudin, K. N.; Strain, M. C.; Farkas, O.; Tomasi, J.; Barone, V.; Cossi, M.; Cammi, R.; Mennucci, B.; Pomelli, C.; Adamo, C.; Clifford, S.; Ochterski, J.; Petersson, G. A.; Ayala, P. Y.; Cui, Q.; Morokuma, K.; Malick, D. K.; Rabuck, A. D.; Raghavachari, K.; Foresman, J. B.; Cioslowski, J.; Ortiz, J. V.; Stefanov, B. B.; Liu, G.; Liashenko, A.; Piskorz, P.; Komaromi, I.; Gomperts, R.; Martin, R. L.; Fox, D. J.; Keith, T.; Al-Laham, M. A.; Peng, C. Y.; Nanayakkara, A.; Gonzalez, C.; Challacombe, M.; Gill, P. M. W.; Johnson, B. G.; Chen, W.; Wong, M. W.; Andres, J. L.; Head-Gordon, M.; Replogle, E. S.; Pople, J. A. *Gaussian 98*; Gaussian, Inc.: Pittsburgh, PA, 1998.
(29) Champion, D. J.; Tomkinson, J.; Kearley, G. J. *Appl. Phys. A* **2002**, *74*, S1302.
(30) Falk, M.; Whalley, E. *J. Chem. Phys.* **1961**, *34*, 1554.
(31) Jobic, H. *Spectrochim. Acta, Part A* **1992**, *48*, 293.
(32) Takano, M.; Sasada, Y.; Satoh, T. *J. Mol. Spectrosc*. **1968**, *26*, 157.
(33) Perchard, J.-P.; Josein, M.-L. *J. Chim. Phys. Phys.-Chim. Biol*. **1969**, *65*, 1834.
(34) Perchard, J.-P.; Josein, M.-L. *J. Chim. Phys. Phys.-Chim. Biol.* **1969**, *65*, 1856.
(35) Eng, J.; Raghavachari, K.; Struck, L. M.; Chabal, Y. J.; Bent, B. E.; Flynn, G. W.; Christman, S. B.; Chaban, Ed E.; Williams, G. P.; Radermacher, K.; Mantl, S. *J. Chem. Phys*. **1997**, *106*, 9889.
(36) Abdurakhmanov, A. A.; Rahimova, R. A.; Imanov, L. M. *Phys. Lett. A* **1970**, *32*, 123.
(37) Fukushima, K.; Zwolinski, B. J. *J. Mol. Spectrosc*. **1968**, *26*, 368, and references there in.
(38) Ohno, K.; Yoshida, H.; Watanabe, H.; Fujita, T.; Matsuura, H. *J. Phys. Chem*. **1994**, *98*, 6924.
(39) Crowder, G. A.; Townsend, M. J. *J. Mol. Struct*. **1977**, *42*, 27.
(40) Gonzalez, L.; Mo, O.; Yanez, M. *J. Chem. Phys*. **1999**, *111*, 3855.
(41) George, W. O.; Has, T.; Hossain, Md. F.; Jones, B. F.; Lewis, R. *J. Chem. Soc., Faraday Trans.* **1998**, *94*, 2701.
(42) Michielsen-Effinger, J. *J. Mol. Spectrosc*. **1969**, *29*, 489.
(43) Barnes, J.; Hallam, H. E. *J. Chem. Soc., Faraday Trans*. **1970**, *66*, 1920.
(44) Sakar, S.; Joarder, R. N. *J. Chem. Phys*. **1994**, *100*, 5118.
(45) Radom, L.; Hehre, W.; Pople, J. A. *J. Am. Chem. Soc*. **1971**, *93*, 289.
(46) Yin, P. K. L.; Rao, K. N. *J. Mol. Spectrosc. Notes* **1968**, 489.
(47) Nelligan, W. B.; LePoir, D. J.; Brun, T. O.; Kleb; R. *J. Phys. Chem.* **1987**, *87*, 2447.
(48) Levitt, L. S.; Widing, H. F. *Prog. Phys. Org. Chem*. **1976**, *12*, 119.
(49) Nitta, T.; Turek, E. A.; Greenkorn, R. A.; Chao, K. C. *AIChE J.* **1977**, *23*, 144.
(50) Gonzalez, D.; Cerdeirina, A. A.; Romani, L.; Carballo, E. *J. Phys. Chem. B* **2000**, *104*, 11275.
(51) Braden, D. A.; Parker, S. F.; Tomkinson, J.; Hudson, B. S. *J. Chem. Phys*. **1999**, *111*, 429.
(52) Carboll, E.; Mosquera, R. A.; Legido, J. L.; Romani, L. *J. Chem. Soc., Faraday Trans*. **1997**, *93*, 3437.
(53) Weng, S. X.; Anderson, A. *Phys. Status Solidi B* **1992**, *172*, 545.
(54) Anderson, A.; Andrews, B.; Meiering, E. M.; Torrie, B. H. *J. Raman Spectrosc*. **1988**, *19*, 85.
(55) Joensson, P. G. *Acta Crystallogr., Sect. B* **1976**, *32*, 232.
(56) Mikawa, Y.; Brasch, J. W.; Jakobsen, R. J. *Spectrochim. Acta, Part A* **1997**, *27*, 529.
(57) Stuart, A. V.; Sutherland, G. B. B. M. *J. Chem. Phys*. **1956**, *24*, 559.
(58) Vogel-Weill, C.; Corset, J. *Spectrochim. Acta, Part A* **1995**, *51*, 2357.
(59) Eder-Mirth, G.; Lercher, J. A. *Recl. Trav. Chim. Pays-Bas* **1996**, *115*, 157.
(60) Vayssilov, G.; Lercher, J. A.; Rösch, N. *J. Phys. Chem. B* **2000**, *104*, 8614.
(61) *CRC Handbook of Chemistry and Physics* 56th ed.; 1975−1976.
(62) Fubini, B.; Bolis, V.; Cavenago, A.; Garrone, E.; Ugliengo, P. *Langmuir* **1993**, *9*, 2712.
(63) Chung, J. S.; Bennett, C. O. *J. Catal*. **1985**, *92*, 173.
(64) Max, J.-J.; Daneault, S.; Chapados, C. *Can. J. Chem.* **2002**, *80*, 113.
(65) Gutmann, V. *The Donor Acceptor Approach to Molecular Interactions*; Plenum Press: New York, 1978.
(66) Anderson, M. W.; Barrie, P. J.; Klinowski, J. *J. Phys. Chem*. **1991**, *95*, 235.
(67) Dubinin, M. M.; Isirikyan, A. A.; Regent, N. I. *Izv. Akad. Nauk. SSSR, Ser. Khim.* **1976**, *2*, 288.